

## Microstructure and mechanical properties of extruded Mg–6Zn–xEr alloys

Ke LIU, Qing-feng WANG, Wen-bo DU, Zhao-hui WANG, Shu-bo LI

School of Materials Science and Engineering, Beijing University of Technology, Beijing 100124, China

Received 6 August 2012; accepted 30 January 2013

**Abstract:** The microstructure and mechanical properties of the Mg–6Zn–xEr alloys in the as-cast, as-extruded and extruded-T5 states were investigated. It is found that the addition of Er has an obvious effect on improving mechanical properties of Mg–6Zn based alloys. The results suggest that the Mg–6Zn–0.5Er alloy in the peak aged state shows the best tensile strength. The ultimate tensile strength and the yield tensile strength of the peak-aged Mg–6Zn–0.5Er alloy are about 329 MPa and 183 MPa, respectively, accompanying with a good elongation of 12%. The addition of 0.5% Er into the Mg–6Zn based alloys has a great effect on improving ageing hardening response. The highest tensile strength of the peak-aged Mg–6Zn–0.5Er alloy is mainly due to the refinement of microstructure and the precipitation of  $\beta_1$  phase.

**Key words:** magnesium alloy; Mg–Zn–Er alloy; hot extrusion; dynamic recrystallization

### 1 Introduction

Magnesium alloys are considered one kind of the most important structural materials because of their high specific strength, good damping capacity and recycle. Significantly, the magnesium resource is so abundant that it can meet the needs for the aircraft, railway and automotive industries in future. The Mg–Zn based alloys are usually considered one of the promising candidate magnesium alloys because of cheap price and obvious ageing hardening. However, the mechanical properties of Mg–Zn binary alloys are low because of the existence of coarse Mg–Zn binary phase. Therefore, the rare earth (RE) elements are generally added in order to improve the mechanical properties of Mg–Zn binary alloys [1–4]. It should be noted that the RE additions always lead to a precipitation of some ternary phases, such as the *W*-phase and the *I*-phase [5–8]. Furthermore, both the *I*-phase and the *W*-phase usually form on the basis of the chemical compositions of the Mg–Zn–RE alloys [9–13]. As reported, the *I*-phase (Mg<sub>3</sub>Zn<sub>6</sub>RE) has good properties, such as high hardness and low surface energy, which are great beneficial to improve the tensile strength [14]. As reported by PARK et al [15], the yield tensile strength of Mg–Zn–Y–Zr alloys is ranging from

150 MPa to 450 MPa at room temperature, depending on the content of the *I*-phase. However, the *W*-phase with a cubic structure is not coherent with the matrix, which is harmful to the mechanical properties [3,9,16,17]. According to the contributions [18–22], the *I*-phase had been found in Mg–Zn–Y, Mg–Zn–Gd, Mg–Zn–Er, Mg–Zn–Ho, Mg–Zn–Dy and Mg–Zn–Tb series alloys.

However, the *I*-phase in as-cast Mg–Zn–RE alloys is usually coarse and distributed uniformly, which leads to an unobvious improvement of mechanical properties. So, thermomechanical process as well as heat treatment is usually adopted to refine the microstructure. The thermomechanical process mainly includes hot extrusion, hot rolling, equal-channel angular pressing and rapidly solidified powders, by which the microstructure is refined greatly, resulting in enhancement of the tensile strength and the elongation obviously [4,19,23–27]. Meanwhile, both the microstructure and the mechanical properties of the as-extruded Mg–Zn–RE alloys have been investigated directly without considering ageing process [4,28,29]. However, it is well known that the Mg–Zn based alloys usually display a better ageing response due to the presence of the  $\beta_1'$  phase [30–33]. Therefore, it may be a possible way to further improve the mechanical properties of Mg–Zn–RE alloys via peak ageing process.

In the present work, microstructure and mechanical properties of Mg–6Zn– $x$ Er (mass fraction, %) alloys ( $x=0.30, 0.50, 1.0, 1.5$  and  $2.0$ , which are identified as alloys A, B, C, D and E) were investigated. The ageing hardening behaviors of as-extruded Mg–6Zn– $x$ Er alloys at  $200\text{ }^{\circ}\text{C}$  with time were studied and the strengthening mechanism in the peak-aged alloys was expatiated.

## 2 Experimental

The alloys with nominal compositions of Mg–6Zn– $x$ Er ( $x=0.30, 0.50, 1.0, 1.5$  and  $2.0$ ) were produced from high-purity Mg (99.5%), high-purity Zn (>99.9%) and Mg–20Er (mass fraction, %) master alloy in an electric resistance furnace at about  $750\text{ }^{\circ}\text{C}$  under a protective atmosphere. The melting in a graphite crucible was poured into an iron mold with dimensions of  $40\text{ mm}\times 100\text{ mm}\times 150\text{ mm}$  at  $720\text{ }^{\circ}\text{C}$ . The as-cast alloy blocks were homogenized at  $400\text{ }^{\circ}\text{C}$  and held for 10 h, and then quenched in  $70\text{ }^{\circ}\text{C}$  water. The homogenized blocks were machined into ingots with a diameter of 35 mm. At last, the ingots were hot extruded into rods indirectly with a extrusion ratio of 10 at  $300\text{ }^{\circ}\text{C}$ . The rods were directly aged at  $200\text{ }^{\circ}\text{C}$  with time in order to investigate ageing hardening responses. Specimens for the tensile test were made into dog-bone with 5 mm in gauge diameter and 25 mm in gauge length. Tensile test was conducted on a DNS–20 uniaxial tensile testing machine at a rate of 1 mm/min. Vickers hardness was measured by a HVS–1000 hardness tester with a load of 2.94 N and a dwelling time of 10 s, and 10 measurements were collected for each sample. Besides, the impact toughness test was carried out on a JB–5 pendulum impact tester (the measurement range of the impact absorbing energy  $A_{kv}$  is 2.45–23.52 J). The impact toughness specimens were made into Charpy V notch type with 55 mm in gauge length, 10 mm in gauge height and 5 mm in gauge width, as shown in Fig. 1. The value of the  $A_{kv}/A$  in the present investigation was the average of three measurements for each kind of alloys, where  $A$  is the cross-sectional area of the specimen.

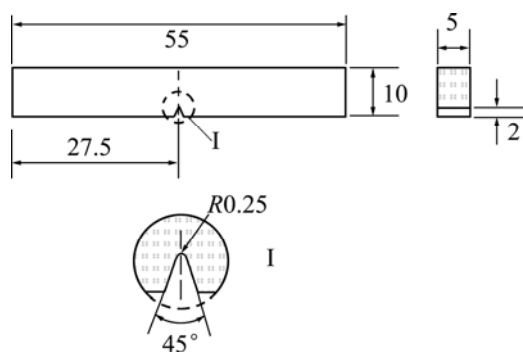


**Fig. 1** Charpy V type notch specimen for impact toughness test (Unit: mm)

The chemical compositions of alloys were analyzed by X-ray fluorescence (XRF) analyzer. The chemical compositions are shown in Table 1. Phase analysis of the alloys was conducted by X-ray diffractometer (XRD). The microstructures of alloys were observed by optical microscope (OM), scanning electron microscope (SEM) equipped with energy dispersive spectroscopy (EDS) and transmission electron microscope (TEM) with selected area electron diffraction (SAED) pattern and EDS. The average grain size of the alloys was measured via the linear intercept method. The samples for OM and SEM observations were mechanically polished and then etched in a solution of 4 mL nitric acid and 96 mL ethanol. Specimens for TEM observation were prepared by electro-polishing and ion beam milling.

**Table 1** Chemical composition of Mg–6Zn– $x$ Er alloys

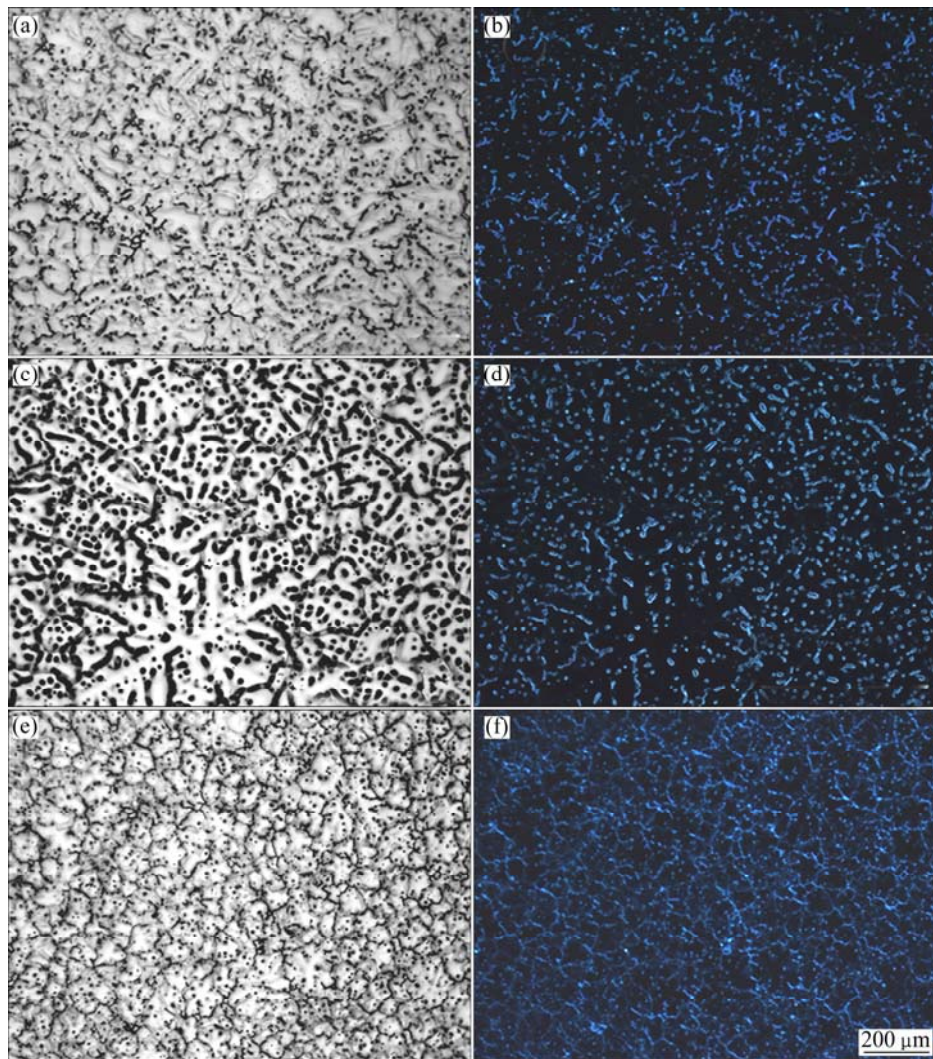
No.	Nominal alloy	Mg	w(Zn)/%	w(Er)/%	w(Zn)/w(Er)
A	Mg–6Zn	Bulk	6.3	–	–
B	Mg–6Zn–0.30Er	Bulk	6.0	0.35	17.1
C	Mg–6Zn–0.50Er	Bulk	6.0	0.53	11.3
D	Mg–6Zn–1.0Er	Bulk	5.5	1.0	5.5
E	Mg–6Zn–1.5Er	Bulk	6.0	1.4	4.3
F	Mg–6Zn–2.0Er	Bulk	5.9	2.1	2.8

## 3 Results

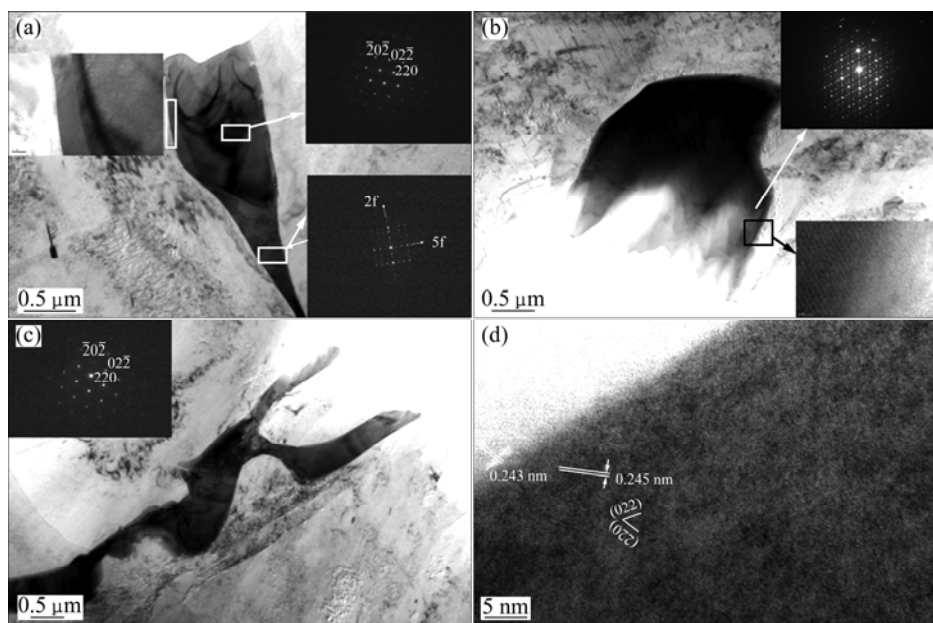
### 3.1 Microstructure of as-cast alloys

Figure 2 shows the OM images of as-cast alloys A, C and E. It suggests that the alloys are composed of dendrites of magnesium matrix as well as the secondary phases. The dendrites are separated by the secondary phases. The morphologies of the secondary phases are closely related with the addition of Er. The morphologies of the secondary phases are transforming from incontinuous network to continuous network as the addition of Er increases. In addition, the volume fraction of the compounds is also improved obviously with increment of Er addition. The XRD test was carried out, which is not shown in the present work. The results suggest that the phase compositions mainly depend on the content of Er in the alloys. When the addition of Er is less than 0.5, the alloys are mainly composed of  $\alpha$ -Mg solid solution together with the secondary phases of  $I$ -phase and  $Mg_7Zn_3$  phase. However, the further increment of Er leads to a precipitation of the  $W$ -phase. The phase constituents of the alloys C, D and E are mainly  $\alpha$ -Mg solid solution,  $I$ -phase and  $W$ -phase.

Figure 3 shows the TEM images obtained from the alloy E. Figure 3(a) shows an interesting result that the  $W$ -phase is surrounded completely by the  $I$ -phase, which has not been found in previous reports. The EDS results imply that the composition of the  $W$ -phase is about

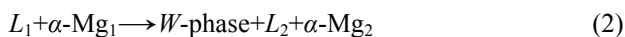


**Fig. 2** OM images of as-cast alloys with bright field (a,c,e) and with dark field (b,d,f): (a,b) Alloy A; (c, d) Alloy C; (e,f) Alloy E

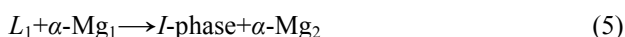


**Fig. 3** TEM images of secondary phases obtained from as-cast Mg-6Zn-2.0Er alloy: (a) *W*-phase surrounded by *I*-phase and corresponding SAED patterns of *W*-phase and *I*-phase, respectively; (b) Block *I*-phase and corresponding SAED pattern; (c) Coarse *W*-phase and corresponding SAED pattern; (d) HRTEM image of interface between matrix and *W*-phase

Mg–39.4Zn–29.6Er (mole fraction, %), and the composition of the *I*-phase is about Mg–56.1Zn–11.7Er (mole fraction, %). Therefore, it indicates that the *I*-phase may be formed by the following equation in the as-cast alloy E [34,35]:



Besides, both the *I*-phase and the *W*-phase which are present separately in the alloy E are found, respectively, as shown in Figs. 3(b) and (c). A separate *I*-phase with a size of  $\sim 3 \mu\text{m}$  is shown in Fig. 3(b). The composition of the *I*-phase is about Mg–62.3Zn–11.4Er (mole fraction, %), and the corresponding SAED pattern shows its own two-fold symmetry (see inset image in Fig. 3(b)). Furthermore, the HRTEM shows that the *I*-phase is coherent with the matrix, as shown in the inset image at the bottom right corner of Fig. 3(b). Meanwhile, it can clearly see that a kind of phase with a rod-like morphology locates near the *I*-phase. According to Refs. [3–6], the rod-like phase may be the  $\beta'_1$  phase which is commonly observed in the peak-aged Mg–Zn based alloys. However, it is generally found that the Mg–Zn phase does not precipitate around the *W*-phase. As shown in Fig. 3(c), a coarse *W*-phase with a size of  $\sim 1 \mu\text{m}$  in width is observed. Around the *W*-phase, we do not find the presence of the Mg–Zn phase obviously. The kind of the Mg–Zn precipitations may be related with the composition of the micro-area around which the coarse secondary phases formed during solidification. Therefore, the EDS test was conducted in order to investigate the composition of the micro-area around the coarse *I*-phase and *W*-phase. The average composition of the micro-area near the *I*-phase is Mg–(2.24 $\pm$ 0.41) Zn (mole fraction, %) while the average composition near the *W*-phase is Mg–(1.22 $\pm$ 0.13) Zn (mole fraction, %). They are the average composition values, and three measurement points are obtained near the *W*-phase and *I*-phase, respectively. This indicates that the micro-area where both the *I*-phase and the Mg–Zn binary phase precipitated have a higher content of Zn. Therefore, it is suggested that the formation of the *I*-phase may obey another reaction equation:



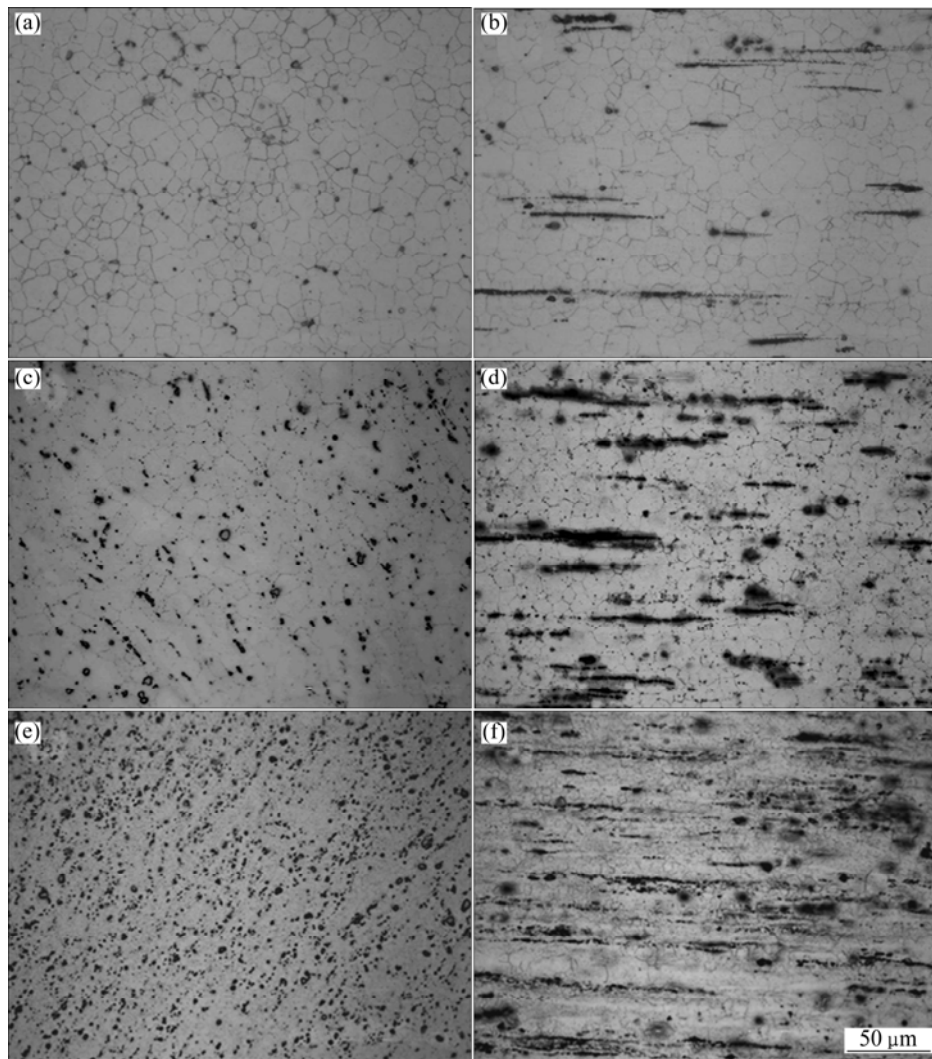
It is well known that the composition of the liquid of the alloys is not static during solidification at atmosphere. Therefore, the composition of micro-areas will be different via releasing solution of Er and Zn. If the composition of the area, where the content of Zn is richer, agrees well with the composition of the *I*-phase, it will result in the formation of the *I*-phase directly.

However, if the composition of the micro-area agrees with the precipitation of *W*-phase well, it will lead to the precipitation of the *W*-phase directly. Besides, if the composition near the precipitation of the *W*-phase is rich in Zn, it will contribute to the formation of the *I*-phase at the interface of the *W*-phase. It is concluded that the formation of the *I*-phase in the as-cast Mg–6Zn–2.0Er alloy is related with the compositions of the micro-area closely. The area where the Zn is richer mostly leads to the precipitation of the *I*-phase. As a result, the precipitation of the *I*-phase can be depicted by the following equations:  $L + \alpha\text{-Mg}_1 \rightarrow I\text{-phase} + \alpha\text{-Mg}_2$ ;  $L + W\text{-phase} \rightarrow I\text{-phase} + \alpha\text{-Mg}$ .

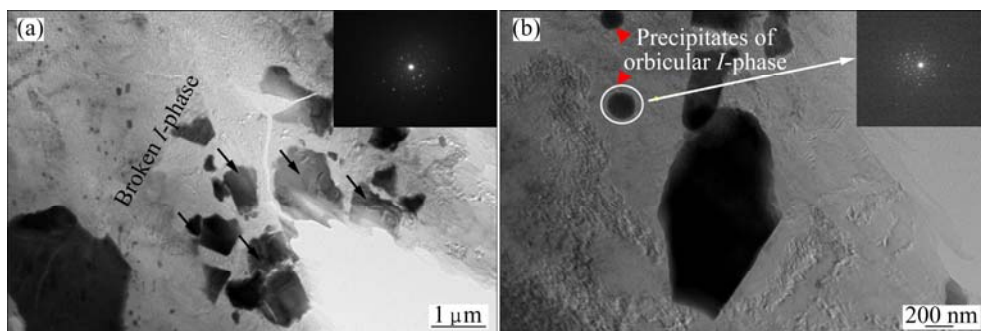
### 3.2 Microstructure of as-extruded alloys

Figure 4 shows the OM images of as-extruded alloys A, B and E. The coarse matrix and the secondary phase were broken instead of fine grains and relative uniform secondary phase. The average grain size of the alloy A is (10.6 $\pm$ 2.0)  $\mu\text{m}$  and the boundaries are clear. A majority of coarse secondary phases were dissolved into the matrix accompanying with the precipitation of lots of tiny particles during hot extrusion. The average grain size of the alloy B is (9.2 $\pm$ 1.9)  $\mu\text{m}$ . The grains tend to be equiaxed. The length of secondary phases is in a range of 0–9.5  $\mu\text{m}$ . The average grain size of the alloy E is (6.9 $\pm$ 1.2)  $\mu\text{m}$ , and the size of the secondary phase is in a range of 0–6  $\mu\text{m}$ . It is suggested that the average grain size of the as-extruded alloys is closely related with the content of Er. The higher addition of Er directly leads to a great deal of Mg–Zn–Er ternary phases, especially in the alloy E. Both the *W*-phase and the *I*-phase are considered main secondary phases, which have high melting points. These phases are still present after homogenization process and hot extrusion process. The thermodynamic stable phase will play an important role in dynamic recrystallization (DRX) via impeding dislocation movements, limiting the growth of both new recrystallized grains and primary grains during hot extrusion. As a result, the microstructure of the alloy E is finer than others after hot extrusion.

Figure 5 shows the TEM images obtained from alloy C. It is found that the coarse secondary phase is broken. Figure 5(a) shows the broken *I*-phase, and its size is 0.5–2  $\mu\text{m}$ . In addition, a new precipitation of particles in a circular morphology is found, as shown in Fig. 5(b). The diameter of the granular particle is about 200 nm, which precipitated during hot extrusion [19,36]. The chemical compositions of the broken *I*-phase and the precipitated circular *I*-phase are Mg–66.4Zn–12.9Er (mole fraction, %) and Mg–23.8Zn–3.92Er (mole fraction, %), respectively. The mole ratio of Zn to Er is closed to 6, which confirms the presence of the *I*-phase.



**Fig. 4** OM images of as-extruded alloys along transverse (extrude) direction (a,c,e) and along longitudinal (extrude) direction (b,d,f): (a, b) Alloy A; (c, d) Alloy B; (e, f) Alloy E



**Fig. 5** TEM images of secondary phases obtained from as-extruded alloy C: (a) Broken *I*-phase; (b) Precipitated *I*-phase during hot extrusion

### 3.3 Ageing hardening behaviors of as-extruded alloys A, B, C, D and E

Figure 6 shows the ageing hardening responses of as-extruded alloys A, B, C, D and E at 200 °C with time. It can be seen that the hardness mostly decreases at the beginning of ageing process, which is mainly due to a

release of stress concentration via growth of grains or formation of new grains/secondary phases. Furthermore, the addition of Er delays the time of peak ageing hardening. The peak hardness of the alloy A is obtained after 5 h, and the peak hardness is about VHN 74. The peak hardness of the alloy B is about VHN 84, which is

obtained after 10 h. The peak hardness of the alloy C is about VHN 74 after 20 h. The peak hardness of the alloy D is about VHN 78 after 15 h. However, the ageing hardening response of the alloy E is unobvious. Conversely, the hardness of the alloy E decreases lightly, and its hardness is about 75 VHN after 25 h. As investigated above, the ageing hardening responses of the alloys generally increase as the addition of Er increases until 0.5%. The addition of 0.5% Er leads to a high ageing hardening response, and the increment of the hardness is about VHN 17 compared with the as-extruded one.

### 3.4 Microstructure of peak-aged alloys

Figure 7 shows the OM images of the peak-aged alloys A, B and E. It indicates that microstructure of the alloys in peak-aged state is different from that of the alloys in as-extruded state. The average grain size of the alloy A is  $(13.1 \pm 2.4) \mu\text{m}$ . This implies that the grain of the alloy A is inclined to grow during isothermal ageing

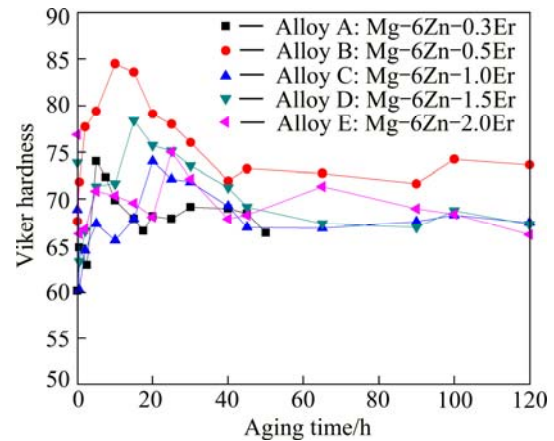


Fig. 6 Ageing hardening responses of as-extruded alloys A, B, C, D and E at 200 °C with time

process. It is mainly due to the few of secondary phases which may play an important role in limiting growth of grains during isothermal ageing process. However,

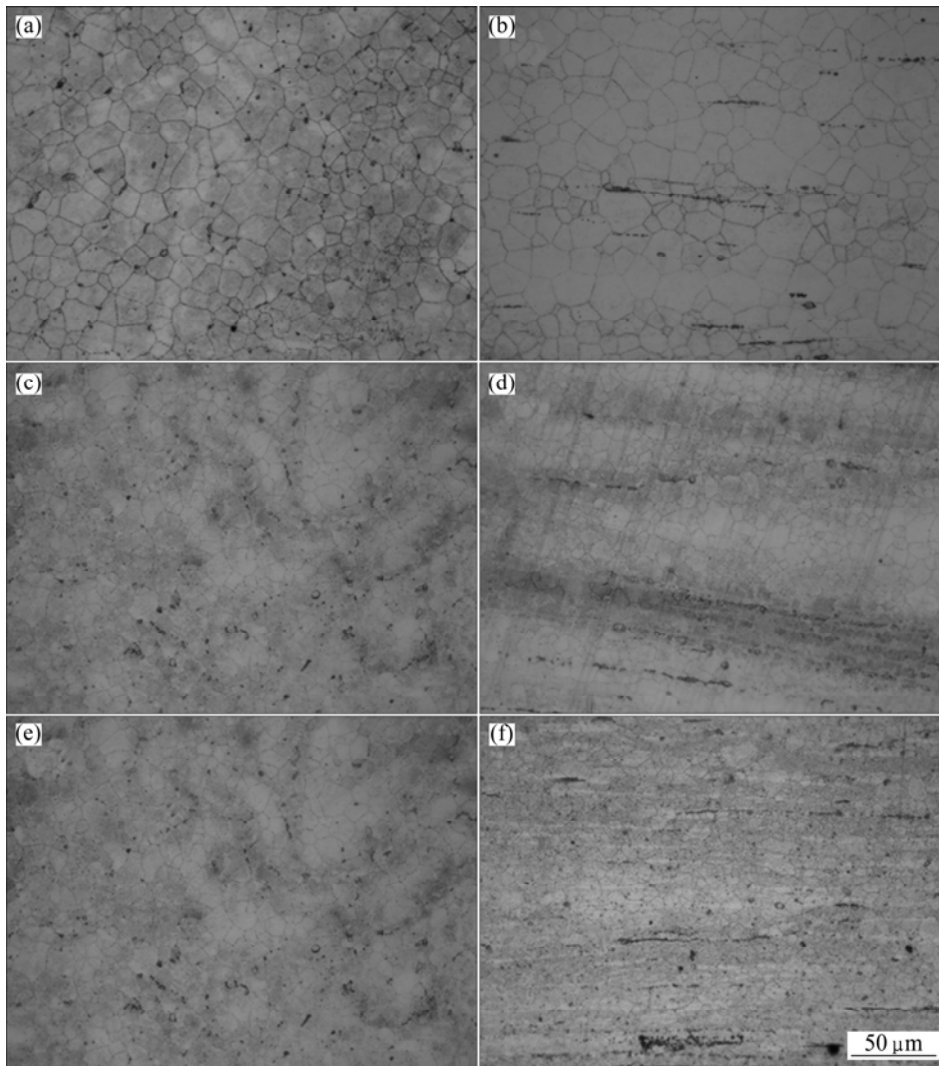


Fig. 7 OM images of peak-aged alloys along transverse (extrude) direction (a,c,e) and along longitudinal (extrude) direction (b,d,f): (a, b) Alloy A; (c, d) Alloy B; (e, f) Alloy E

the average grain sizes of the alloys B and E are  $(8.9 \pm 1.6) \mu\text{m}$  and  $(5.3 \pm 2.1) \mu\text{m}$ , respectively. It should be noted that the average grain sizes of the alloys B and E after peak-aged process become smaller compared with the alloys in the as-extruded state. It is well known that the DRX usually happens in magnesium alloys during hot extrusion because of accumulation of the dislocations [37,38]. However, the DRX is not complete during hot extrusion process. As a result, the remaining stress will continue to be released via formation of subgrain structure or precipitation of secondary phases during ageing process [37,38]. The subgrain structures formed over the whole volume of the grains, and the subgrain structures grew via swallowing the primary grains. Therefore, the grain sizes of alloys B and E after peak ageing process decrease compared with the as-extruded one.

Figure 8 shows the TEM images obtained from the peak-aged alloys B and C. It can be seen that the main precipitation in both of the alloys is the rod-like  $\beta'_1$  phase besides some blocky phases [32,39]. The size of the rod-like  $\beta'_1$  phase in the alloy B is 50–300 nm in length along the  $[0001]_a$  direction and 5–15 nm in width, as shown in Fig. 8(a). The number density of the rod-like  $\beta'_1$  phase is about  $7.5 \times 10^{13} \text{ m}^{-2}$ . However, the size of the  $\beta'_1$  phases in the alloy C is larger than that in the alloy B (see Fig. 8(c)). The size of the rod-like  $\beta'_1$  phase in the alloy C is 75–500 nm in length and 10–20 nm in width. The number density of the rod-like  $\beta'_1$  phase is

about  $1.8 \times 10^{13} \text{ m}^{-2}$ . Therefore, the ageing hardening response of the alloy B is more obvious than that of the alloy C due to the higher density and the smaller size of the  $\beta'_1$  phase. Additionally, a few of elliptical particles are seen in TEM images. The SAED patterns suggest that the elliptical particles may be the *I*-phase, which precipitated during hot extrusion [19,36]. The chemical compositions of the nano-scale *I*-phases shown in Figs. 8(a) and (c) are Mg–25.92Zn–4.77Er (mole fraction, %) and Mg–45.85Zn–10.22Er (mole fraction, %), respectively.

### 3.5 Tensile properties of as-cast, as-extruded and peak-aged alloys at room temperature

In the present work, the tensile properties of the as-cast Mg–6Zn alloy work were studied. However, the as-extruded Mg–6Zn alloy cannot be produced by hot extrusion indirectly at 300 °C because of hot crack. So, Table 2 shows the tensile properties of the alloys A, B, C, D and E in both as-cast and as-extruded states as well as the as-cast Mg–6Zn alloy at room temperature.

As shown in Table 2, the results indicate that the mechanical properties of the as-cast alloys are improved with addition of Er. Significantly, the addition of 1.0% Er results in superior mechanical properties, and the ultimate tensile strength (UTS) and yield tensile strength (YTS) of the as-cast alloy C are about 224 MPa and 104 MPa, respectively, with an elongation of 11%. However, the as-cast alloy E displays the highest YTS among all of

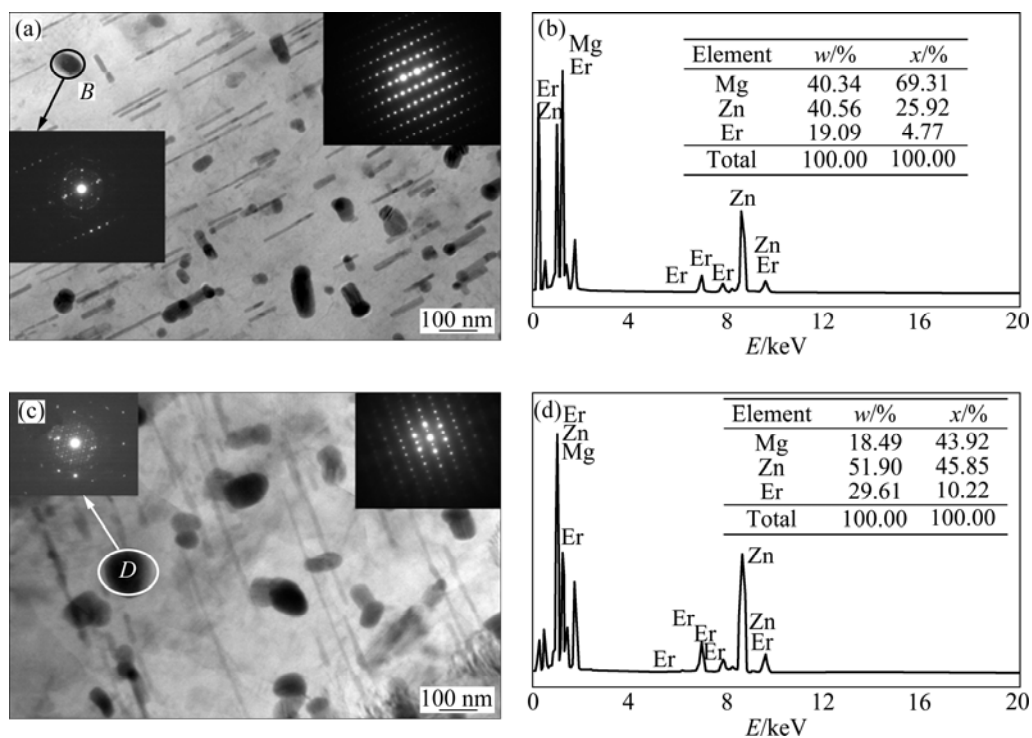


**Fig. 8** TEM images of peak-aged alloys: (a) Precipitates in peak-aged alloy B and corresponding SAED patterns; (b) EDS result of *I*-phase in alloy B; (c) Precipitates in peak-aged alloy C and corresponding SAED patterns; (d) EDS result of *I*-phase in alloy C

**Table 2** Tensile properties of alloys in as-cast and as-extruded states as well as as-cast Mg–6Zn alloy at room temperature

Alloy	State	UTS/ MPa	YTS/ MPa	Elongation/ %
Mg–6Zn	As-cast	170	63	6
Mg–6Zn–0.3Er	As-cast	210	72	12
	As-extruded	289	138	25
Mg–6Zn–0.5Er	As-cast	184	87	12
	As-extruded	310	155	17
Mg–6Zn–1.0Er	As-cast	224	104	11
	As-extruded	295	187	18
Mg–6Zn–1.5Er	As-cast	203	100	10
	As-extruded	296	175	17
Mg–6Zn–2.0Er	As-cast	198	110	6
	As-extruded	304	194	16

the as-cast alloys, and the YTS is about 110 MPa while its elongation is about 6.0%. This suggests that the presence of a high volume fraction of the coarse *W*-phase leads to a failure early during deformation at room temperature.

Hot extrusion process has a great effect on improving mechanical properties. The as-extruded alloy B displays its higher UTS of about 310 MPa. However, a better YTS of about 194 MPa is obtained in as-extruded alloy E. It should be noted that the elongations of the alloys A, B, C, D and E are improved greatly after hot extrusion, which is mainly due to the refinements of microstructure. On the whole, the as-extruded alloy E has more attractive tensile properties compared with others, and the UTS and elongation are about 304 MPa and 16%, respectively.

Table 3 shows the tensile properties of the peak-aged alloys A, B, C, D and E at room temperature. The tensile strength of the alloy B is improved obviously after peak ageing process. The UTS and YTS are 329 MPa and 183 MPa, respectively, with an elongation of 12%. However, the tensile strength of alloys C, D and E is not enhanced significantly. When the addition of Er is more than 1.0%, the tensile strength of the alloys after peak ageing is not heightened greatly. The UTS and YTS of peak-aged alloy C are about 302 MPa and 193 MPa, respectively, accompanying with an elongation of 14%. Furthermore, the tensile strength of the alloy E decreases

**Table 3** Tensile properties of peak-aged alloys A, B, C, D and E at room temperature

Alloy	UTS/MPa	YTS/MPa	Elongation/%
Mg–6Zn–0.3Er	291	157	18%
Mg–6Zn–0.5Er	329	183	12%
Mg–6Zn–1.0Er	302	193	14%
Mg–6Zn–1.5Er	300	188	15%
Mg–6Zn–2.0Er	301	193	12%

after peak ageing, and the UTS and YTS are only 301 MPa and 193 MPa, respectively.

Table 4 shows the impact toughness of the alloys Mg–6Zn–0.5Er and Mg–6Zn–1.0Er in both as-extruded and peak-aged states at room temperature, respectively. It indicates that the higher content of the Er leads to an improvement of the impact toughness. As shown in Table 4, the impact toughnesses of as-extruded alloys Mg–6Zn–0.5Er and Mg–6Zn–1.0Er are  $\sim 11.49$  J/cm<sup>2</sup> and 15.63 J/cm<sup>2</sup>, respectively. Meanwhile, the impact toughness decreases after peak ageing treatment. The tendency of the impact toughness is inverse of that of the tensile property after peak ageing treatment. The impact toughnesses of peak-aged alloys Mg–6Zn–0.5Er and Mg–6Zn–1.0Er are  $\sim 11.16$  J/cm<sup>2</sup> and 9.41 J/cm<sup>2</sup>, respectively. The great decrease in impact toughness of the Mg–6Zn–1.0Er alloy may ascribe to the precipitation of the coarse  $\beta'_1$  phase, as shown in Fig. 8(c).

**Table 4** Impact toughness of Charpy V type notch specimens

Alloy	State	$A_{kv}$ /J	$A_{kv2}$ /(J·cm <sup>-2</sup> )
Mg–6Zn–0.5Er	As-extruded	4.60	11.49
	Peak-aged	4.46	11.16
Mg–6Zn–1.0Er	As-extruded	6.25	15.63
	Peak-aged	3.76	9.41

As stated above, the addition of Er has a great influence on improving the mechanical properties of Mg–6Zn based alloys. Especially, the addition of Er leads to a large enhancement in YTS. The mechanical properties of the alloys are further promoted after hot extrusion, especially the improvement in the elongation. However, the tensile strength does not show a great difference among them. The mechanical properties of the as-extruded alloys after peak ageing process are not improved obviously except the as-extruded alloy B. The alloy B displays a better ageing hardening response and tensile strength after peak ageing process due to the precipitation of the  $\beta'_1$  phase. However, the coarse  $\beta'_1$  phase in the alloy C in peak-aged condition may result in a great decrease in impact toughness.

## 4 Discussion

According to Ref. [10], when the mass ratio of Zn to Er is in a range of 6–10, the main ternary phase in Mg–Zn–Er series alloys was the *I*-phase that had a great effect on improving mechanical properties due to a close coherent interface between the *I*-phase and the  $\alpha$ -Mg [4]. Therefore, the alloys A and B in the as-cast state displayed good tensile properties including a high UTS and a good elongation, compared with Mg–6Zn alloy. However, when the addition of Er is more than 1.0%, the

*W*-phase was present. As reported, the *W*-phase had an FCC (face-centered cubic) structure and it accounted for the decrement of mechanical properties [16,28]. In the present work, the inferior elongation of the alloy E in as-cast state was mainly ascribed to the presence of quantities of *W*-phase mostly.

The alloys A, B, C, D and E exhibited good mechanical properties after hot extrusion [19]. However, the more Er was added, the less content of Zn in the matrix was left, which resulted in the decrement of critical resolved shear stress for basal slip of Mg-based alloys [40]. The solid solution strengthening effect of Zn would be reduced with increasing Er. It is interesting to note that the microstructure of the alloys in as-extruded state was refined mostly due to the DRX during hot extrusion. In addition, the quantities of ternary phases had a great important effect on activating DRX and limiting the grain growths. As a result, the grain size of the alloy E in the as-extruded state was the smallest. According to the Hall–Petch relationship, the YTS would be improved with decreasing grain size. So, the consumption of strength would be compensated by the refinement of microstructure. Therefore, the as-extruded alloy E exhibited a better YTS of 194 MPa companying with a high elongation of 16%.

It has been reported that the precipitation sequence from a supersaturated solid solution (SSSS) in the Mg–Zn based alloys was generally as SSSS→solute clusters→GP zones→ $\beta'_1$  phase (rod-like and blocky-like compounds)→ $\beta'_1$  phase (coarse plates and laths)→ $\beta$  equilibrium phase. The peak-ageing was mainly ascribed to the presence of the rod-like  $\beta'_1$  phase. The main strengthening phase in peak-aged alloys was the rod-like  $\beta'_1$  phase. The  $\beta'_1$  phase precipitated densely and uniformly during ageing process if the content of Zn in the matrix was high enough. However, the addition of Er led to a reduction of Zn in the matrix via transforming *I*-phase/*W*-phase and depressing the solid solubility of Zn. The results suggested that the volume fraction of Mg–Zn–Er ternary phases increased with the addition of Er increasing. As a result, the content of Zn left in the matrix got lower and lower, which suppressed the precipitation of the  $\beta'_1$  phase. So, the as-extruded alloys C, D and E did not show peak ageing hardening obviously. The similar results were reported by YANG et al [16]. Additionally, the results suggested that 0.5% Er was suitable to improve the ageing hardening responses of the Mg–6Zn based alloys. Besides, the alloy containing 0.5% Er after peak-ageing exhibited the best tensile strength. The better tensile properties of the alloy B containing 0.5% Er after peak ageing process were mainly accounted for by refinement of microstructure, precipitation of the  $\beta'_1$  phase and

dispersion of the broken *I*-phase. However, compared with the alloy B, the alloy A with 0.3% Er did not show obvious ageing hardening response and the time to peak ageing was short. Although the content of Zn in the matrix of alloy A was high, the trace of Er addition may not depress the solid solution of Zn in Mg effectively. As a result, the  $\beta'_1$  phase precipitated rapidly and then got coarse fast, which did not result in a significant improvement in ageing hardening responses [31,33]. Besides, the grain of the alloy A was easier to be coarse during hot extrusion and isothermal ageing process, which was harmful to improve the tensile strength. Therefore, addition of 0.5% Er into Mg–6Zn based alloys was suitable to get a as-extruded alloy which had good mechanical properties and ageing response.

## 5 Conclusions

1) The formation of the *I*-phase which was precipitated during solidification obeys two kinds of equations:  $L+W\text{-phase}\rightarrow I\text{-phase}+\alpha\text{-Mg}$ ;  $L+\alpha\text{-Mg}_1\rightarrow I\text{-phase}+\alpha\text{-Mg}_2$ . However, the area near the *I*-phase usually has a higher content of Zn than the area in which the *W*-phase precipitates.

2) The hot extrusion process plays an important role in refining microstructure of Mg–6Zn–*x*Er alloys. Additionally, the average grain size of the as-extruded alloy decreases with increasing Er addition. The as-extruded alloy containing 2.0% Er has the smallest grain, and the size of grain is about 6.89  $\mu\text{m}$ .

3) The as-extruded alloy containing 0.5% Er presents better ageing hardening response at 200 °C with time. The tensile strength of the alloy after peak ageing process is advanced, and the UTS and YTS are about 329 MPa and 183 MPa, respectively.

## References

- [1] WANG Qing-feng, LI Han, LI Shu-bo, WANG Zhao-hui, DU Wen-bo. Microstructure evolution and mechanical properties of extruded Mg–12Zn–1.5Er alloy [J]. Transactions of Nonferrous Metals Society of China, 2011, 21(s): s874–s879.
- [2] LE Qi-chi, ZHANG Zhi-qiang, SHAO Zhi-wen, CUI Jian-zhong, XIE Yi. Microstructures and mechanical properties of Mg–2%Zn–0.4%RE alloys [J]. Transactions of Nonferrous Metals Society of China, 2010, 20(s): s352–s356.
- [3] SINGH A, TSAI A P. On the cubic W phase and its relationship to the icosahedral phase in Mg–Zn–Y alloys [J]. Ser Mater, 2003, 49: 143–148.
- [4] BAE D H, KIM S H, KIM D H, KIM W T. Deformation behavior of Mg–Zn–Y alloys reinforced by icosahedral quasicrystalline particles [J]. Acta Mater, 2002, 50: 2343–2356.
- [5] PADEZHNOVA E M, MILIYEVSKIY E V, DOBATKINA T V, KINZHIBAO V V. Investigation of the Mg–Zn–Y system [J]. Russ

- Metall (Metally), 1982, 4: 185–188.
- [6] LUO Z P, ZHANG S Q. Comment on the so-called Z-phase in magnesium alloys containing zinc and rare-earth elements [J]. *J Mater Sci Lett*, 1993, 12: 1490–1492.
- [7] ABE E, KAWAMURA Y, HAYASHI K, INOUE A. Long-period ordered structure in a high-strength nanocrystalline Mg–1at% Zn–2at% Y alloy studied by atomic-resolution Z-contrast STEM [J]. *Acta Mater*, 2002, 50: 3845–3857.
- [8] LIU K, ZHANG J H, ROKHLIN L L, ELKIN F M, TANG D X, MENG J. Microstructures and mechanical properties of extruded Mg–8Gd–0.4Zr alloys containing Zn [J]. *Mater Sci Eng A*, 2009, 505: 13–19.
- [9] XU D K, TANG W N, LIU L, XU Y B, HAN E H. Effect of Y concentration on the microstructure and mechanical properties of as-cast Mg–Zn–Y–Zr alloys [J]. *J Alloys Compd*, 2007, 432: 129–134.
- [10] LI H, DU W B, LI S B, WANG Z H. Effect of Zn/Er weight ratio on phase formation and mechanical properties of as-cast Mg–Zn–Er alloys [J]. *Mater Des*, 2012, 35: 259–265.
- [11] ZHANG Y, ZENG X Q, LIU L F, LU C, ZHOU H T, LI Q. Effects of yttrium on microstructure and mechanical properties of hot-extruded Mg–Zn–Y–Zr alloys [J]. *Mater Sci Eng A*, 2004, 373: 320–327.
- [12] LUO Su-qin, TANG Ai-tao, PAN Fu-sheng, SONG Kai, WANG Wei-qing. Effect of mole ratio of Y to Zn on phase constituent of Mg–Zn–Zr–Y alloys [J]. *Transactions of Nonferrous Metals Society of China*, 2011, 21(s): s795–s800.
- [13] LEE J Y, KIM D H, LIM H K, KIM D H. Effects of Zn/Y ratio on microstructure and mechanical properties of Mg–Zn–Y alloys [J]. *Mater Lett*, 2005, 59: 3801–3805.
- [14] PIERCE F S, POON S J, GUO Q. Electron localization in metallic quasicrystals [J]. *Science*, 1993, 261: 737–739.
- [15] PARK E S, YI S, OK J B, BAE D H, KIM W T. Solidification and microstructure control of Mg-rich alloys in the Mg–Zn–Y ternary system [J]. *Proceedings of the MRS Fall Meeting [C]/Boston, MA*, 2001.
- [16] YANG J, WANG L D, WANG L M, ZHANG H J. Microstructure and mechanical properties of the Mg–4.5Zn–xGd (x=0, 2, 3 and 5) [J]. *J Alloys Compd*, 2008, 459: 274–280.
- [17] LIU K, ZHANG J H, LU H Y, TANG D X, ROKHLIN L L, ELKIN F M, MENG J. Effect of the long periodic stacking structure and W-phase on the microstructures and mechanical properties of the Mg–8Gd–xZn–0.4Zr alloys [J]. *Mater Des*, 2010, 31: 210–219.
- [18] LUO Z P, ZHANG S, TANG Y, ZHAO D. Quasicrystals in as-cast Mg–Zn–RE alloys [J]. *Scr Metall*, 1993, 28: 1513–1518.
- [19] LIU Y, YUAN G Y, LU C, DING W J. Stable icosahedral phase in Mg–Zn–Gd alloy [J]. *Scr Mater*, 2006, 55: 919–922.
- [20] LI J H, DU W B, LI S B, WANG Z H. Tensile and creep behaviors of Mg–5Zn–2.5Er alloy improved by icosahedral quasicrystal [J]. *Mater Sci Eng A*, 2010, 527: 1255–1259.
- [21] YOSHIDA T, ITOH K, TAMURA R, TAKEUCHI S. Plastic deformation and hardness in Mg–Zn–(Y, Ho) icosahedral quasicrystals [J]. *Mater Sci Eng A*, 2000, 294–296: 748–752.
- [22] HEGGEN M, FEUERBACHER M, SCHALL P, KLEIN H, FISHER I R, CANFIELD P C, URBAN K. Plasticity of icosahedral Zn–Mg–Dy single quasicrystals [J]. *Mater Sci Eng A*, 2000, 294–296: 781–785.
- [23] ZHANG J, MA Q, PAN F S. Effects of trace Er addition on the microstructure and mechanical properties of Mg–Zn–Zr alloy [J]. *Mater Des*, 2010, 31: 4043–4049.
- [24] LEE J Y, LIM H K, KIM D H, KIM W T, KIM D H. Effect of volume fraction of quasicrystal on the mechanical properties of quasicrystal-reinforced Mg–Zn–Y alloys [J]. *Mater Sci Eng A*, 2007, 449–451: 987–990.
- [25] YANG Wen-peng, GUO Xue-feng. High strength magnesium alloy with  $\alpha$ -Mg and W-phase processed by hot extrusion [J]. *Transactions of Nonferrous Metals Society of China*, 2011, 21(11): 2358–2364.
- [26] ZHENG M Y, QIAO X G, XU S W, WU K, KAMADO S, KOJIMA Y. In-situ quasicrystal-reinforced magnesium matrix composite processed by equal-channel-angular-extrusion [J]. *J Mater Sci*, 2005, 40: 2587–2590.
- [27] MÜLLER A, GARCÉS G, PÉREZ P, ADEVA P. Grain refinement of Mg–Zn–Y alloy reinforced by an icosahedral quasicrystalline phase by severe hot rolling [J]. *J Alloys Compd*, 2007, 443: L1–L5.
- [28] XU D K, LIU L, XU Y B, HAN E H. Effect of microstructure and texture on the mechanical properties of the as-extruded Mg–Zn–Y–Zr alloys [J]. *Mater Sci Eng A*, 2007, 443: 248–256.
- [29] WANG J F, GAO S, SONG P F, HUANG X F, SHI Z Z, PAN F S. Effects of phase composition on the mechanical properties and damping capacities of as-extruded Mg–Zn–Y–Zr alloys [J]. *J Alloys Compd*, 2011, 509: 8567–8572.
- [30] CHUN J S, BYRNE J G. Precipitate strengthening mechanisms in magnesium zinc alloy single crystals [J]. *J Mater Sci*, 1969, 4: 861–872.
- [31] WEI L Y, DUNLOP G L, WESTENGEN H. Precipitation hardening of Mg–Zn and Mg–Zn–RE alloys [J]. *Metall Mater Trans*, 1995, 26: 1705–1716.
- [32] GENG J, GAO X, FANG X Y, NIE J F. Enhanced age-hardening response of Mg–Zn alloys via Co additions [J]. *Scr Mater*, 2011, 64: 506–509.
- [33] BUHA J. Grain refinement and improved age hardening of Mg–Zn alloy by a trace amount of V [J]. *Acta Mater*, 2008, 56: 3533–3542.
- [34] LEBRUN N, STAMOU A, BAETZNER C, ROBINSON J. PETZOW G, EFFENBERG E. Magnesium-yttrium-zinc in ternary phase diagrams [M]. Weinheim, FGR: VCH Verlagsgesellschaft, 1988: 702–710.
- [35] SINGH A, SOMEKAWA H, MUKAI T. High temperature processing of Mg–Zn–Y alloys containing quasicrystal phase for high strength [J]. *Mater Sci Eng A*, 2011, 528: 6647–6651.
- [36] MORA E, GARCÉS G, OÑORBE E, PÉREZ P, ADEVA P. High-strength Mg–Zn–Y alloys produced by powder metallurgy [J]. *Scr Mater*, 2009, 60: 776–779.
- [37] YANG Z, GUO Y C, LI J P, HE F, XIA F, LIANG M X. Plastic deformation and dynamic recrystallization behaviors of Mg–5Gd–4Y–0.5Zn–0.5Zr alloy [J]. *Mater Sci Eng A*, 2008, 485: 487–491.
- [38] TAN J C, TAN M J. Dynamic continuous recrystallization characteristics in two stage deformation of Mg–3Al–1Zn alloy sheet [J]. *Mater Sci Eng A*, 2003, 339: 124–132.
- [39] GAO X, NIE J F. Characterization of strengthening precipitate phases in a Mg–Zn alloy [J]. *Scr Mater*, 2007, 56: 645–648.
- [40] CÁCERES C H, BLAKE A. The strength of concentrated Mg–Zn solid solutions [J]. *Phys Stat Sol A*, 2002, 194: 147–158.

## 挤压态 Mg-6Zn-xEr 合金的微观结构和力学性能

刘 轲, 王庆峰, 杜文博, 王朝辉, 李淑波

北京工业大学 材料科学与工程学院, 北京 100124

**摘 要:** 研究铸态、挤压态和挤压峰值态的 Mg-6Zn-xEr 合金的微观组织和力学性能。结果表明, Er 的加入可显著改善 Mg-6Zn 合金的力学性能, 经过峰值时效后合金的力学性能得到进一步提高; 挤压态 Mg-6Zn-0.5Er 合金经过峰值时效处理后具有最佳的拉伸强度。该合金的抗拉强度和屈服强度分别为 329 MPa 和 183 MPa, 伸长率为 12%。这表明添加 0.5% Er 可显著提高 Mg-6Zn 合金的时效硬化行为。挤压峰值态 Mg-6Zn-0.5Er 合金较好的力学性能归因于结构的细化和  $\beta_1'$  相的析出强化。

**关键词:** 镁合金; Mg-Zn-Er 合金; 热挤压; 动态重结晶

(Edited by Xiang-qun LI)